A Mobile Mapping Solution for VRU Infrastructure Monitoring via Low-Cost LiDAR-Sensors

MARIO ILIC, JOHANNA VOGT AND KLAUS BOGENBERGER

Chair of Traffic Engineering and Control • Technical University of Munich • Arcisstraße 21 • 80333 Munich

Tel.: +49 (0)89 289 22438 • E-Mail: mario.ilic@tum.de

Word count (without references, headers and table/figure captions): 2990 words

Keywords: Low-Cost LiDAR Sensor, VRU Infrastructure Mapping, Mobile 3D Mapping, Urban Data Mining

Summary: *LiDAR scanning of infrastructure is a well-known method to obtain accurate information about roads and their condition. Scanning with this type of sensor is expensive and usually only covers the quality of vehicular infrastructure. Infrastructure for Vulnerable Road Users (VRUs), such as pedestrians or cyclists, is often neglected. Thanks to ever-improving electronics, it is now possible to incorporate high-performance LiDAR sensors made of conventional semiconductor materials into mobile devices. The following article illustrates various experiments with an iPad Pro 2020 LiDAR sensor for low-cost mobile mapping of VRU infrastructure. Using the "3D Scanner App", detailed and qualitative point clouds can be created at low speed levels. In addition, potholes and bumps perpendicular to the road can be detected with remarkable accuracy. This fact enables various mobile mapping solutions for VRU infrastructure monitoring, such as a crowd-sourcing option for urban data mining or an interface to urban digital twins, at a much lower cost than conventional sensor solutions.*

Introduction

Scanning infrastructure with LiDAR (light detection and ranging) sensors is a proven method to obtain precise measurement data of roads and their conditions (Puente, González-Jorge, Arias, & Armesto, 2011). However, high quality LiDAR sensors are immensely expensive to purchase. Due to advancing digitalisation and ever-improving electronics, it is possible to produce inexpensive LiDAR sensors using conventional semiconductor materials (Dummer, Johnson, Rothwell, Tatah, & Hibbs-Brenner, 2021). These LiDAR sensors, which use diodes as lasers and detectors, can also be installed in mobile devices due to their immensely small build. Since 2020, both the Apple iPhone 12 and the iPad Pro 2020 have incorporated a LiDAR sensor (Apple, 2020). The availability of such sensor systems in mobile devices enables the participation of pedestrians and cyclists in urban data mining, not just vehicles being equiped with such sensor technology. Considering the increasing strategic focus of municipalities and cities towards encironmentaly friendly and active modes of transportation, this opens up new potentials for sustainable and citizen-oriented urban planning.

In (Vogt, Rips, & Emmelmann, 2021), Apple's LiDAR sensor was compared with an industrial 3D scanner, with the result that the LiDAR sensor from Apple can be a good choice depending on the application. Suitability tests of the LiDAR sensors of the iPhone 12 Pro and the iPad Pro 2020 can be found in literature. In the research areas of Earth Science (Luetzenburg, Kroon, & Bjørk, 2021), Forest Inventory (Gollob, Ritter, Kraßnitzer, Tockner, & Nothdurft, 2021), Geoscience Fieldwork (Tavani, et al., 2021) and Architectual Surveying (Spreafico, Chiabrando, Losè, & Tonolo, 2021) Apple's LiDAR sensor was primarily used to scan static objects.

In the following paper, various experiments are conducted to test the extent to which the LiDAR sensor built into the Apple iPad Pro 2020 can be used to map infrastructure in a mobile and cost-effective way. The experiments are performed from the perspective of VRUs, in particular cyclists and pedestrians, showing that the limitations of the sensor's handling are outweighed by its versatility and by being a cost-effective alternative to established techniques and traditional approaches.

Methodology

In general, a LiDAR sensor emits laser pulses and detects their reflection. The duration from emission to detection of the laser pulse is decisive. From this, an exact distance is calculated, which, repeated several times, results in a three-dimensional point cloud. The LiDAR sensor used by Apple in its iPad Pro 2020 consists of VCSEL diodes from Lumentum as the laser, while the detector consists of an array of SPAD diodes from Sony. Those two types of diodes can be manufactured using conventional semiconductor manufacturing techniques. This combination drastically simplifies the traditional LiDAR design, allowing for a smaller size and relatively low purchase costs. The LiDAR scanner of the iPad Pro 2020 operates at a wavelength of 8XX nm, has a range of approximately 5 metres and a limited field of view due to its inability to rotate. (Rangwala, 2020)

The app used was the free "3D Scanner App" from Laan Labs (labs.laan.com), downloaded from the Apple iStore. According to Apple, the data from the LiDAR sensor is compressed together with camera data and motion sensor data and then improved by a "computer vision algorithm". The generated point cloud can be exported in different output formats.

In order to test the suitability of the LiDAR sensor built into the iPad Pro 2020 for the purpose of a mobile mapping service, various tests were carried out. Tab. 1 categorises the test characteristics into three areas: Sensor Alignment, Resolution and Speed Level. Whenever the term sensor is used in the following, it always refers to the LiDAR sensor in the iPad Pro 2020.

<table>
<tr><th></th><th>Sensor Alignment</th><th>Resolution</th><th>Speed Level</th></tr>
<tr><td rowspan="5">Bicycle-mounted Sensor
(see Fig. 1, (a))</td><td rowspan="2">Frontal (Position 1)</td><td>High</td><td rowspan="2">Moderate
(Cycling, approx. 15 km/h)</td></tr>
<tr><td rowspan="4">Low</td></tr>
<tr><td>Fully Lateral (Position 2)</td></tr>
<tr><td>Partially Lateral (Position 3)</td><td>Low
(Walking, approx. 5 km/h)</td></tr>
<tr><td>Dynamic Swivelling (Position 4)</td><td>Stationary (0 km/h)</td></tr>
<tr><td>Static Swivelling (Position 4)</td></tr>
<tr><td rowspan="2">Handheld Sensor
(see Fig. 1, (b))</td><td>Dynamic, Semi-Perpendicular (Position 1)</td><td rowspan="2">Low</td><td>Low
(Walking, approx. 5 km/h)</td></tr>
<tr><td>Static, Fully Perpendicular (Position 2)</td><td>Stationary (0 km/h)</td></tr>
</table>

Tab. 1: Test characteristics for the different experimental setups

In order to test the general suitability of the LiDAR sensor for mobile infrastructure mapping, it was mounted on a bicycle in various orientations. Scans were taken in each of these orientations and compared with each other. The different sensor alignments are shown in Fig. 1 (a). In order to determine an optimal alignment of the sensor on the bicycle, frontal and lateral (fully and partially) orientations were tested. In addition, static and dynamic swivelling of the sensor was used to assess the recording capabilities in horizontal direction.

Furthermore, tests were carried out to detect individual infrastructural damages. For this purpose, the sensor, or respectively the iPad Pro 2020, was held in the hand for scanning (Fig. 1 (b)). Two different alignments of the iPad were examined for the tests on foot. The iPad was held semi-perpendicular and fully perpendicular for scanning.

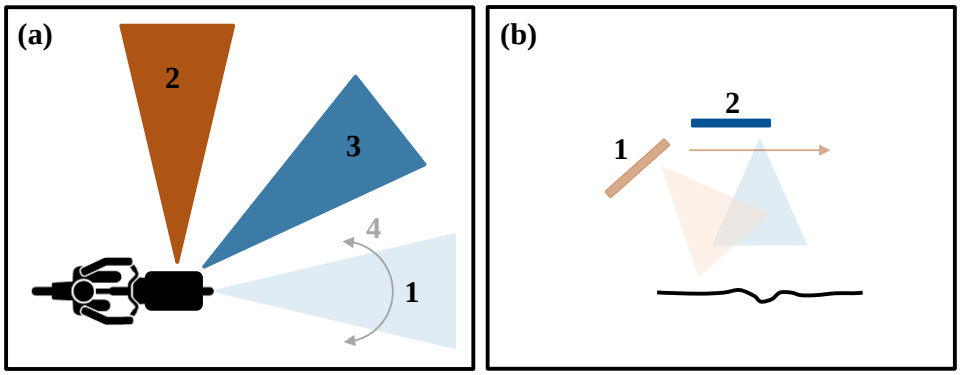

Fig. 1: Sensor Alignments for the different experimental setups

The "3D Scanner App" used for the tests had two different resolution settings: low resolution and high resolution. Three speed levels were examined to find out at which speed the sensor can still generate high-quality point clouds. The chosen gradations were: moderate cycling at approx. 15 km/h, walking at approx. 5 km/h and stationary (0 km/h).

All tests were carried out in dry, windless and sunny weather conditions on the test track shown in Fig. 2.

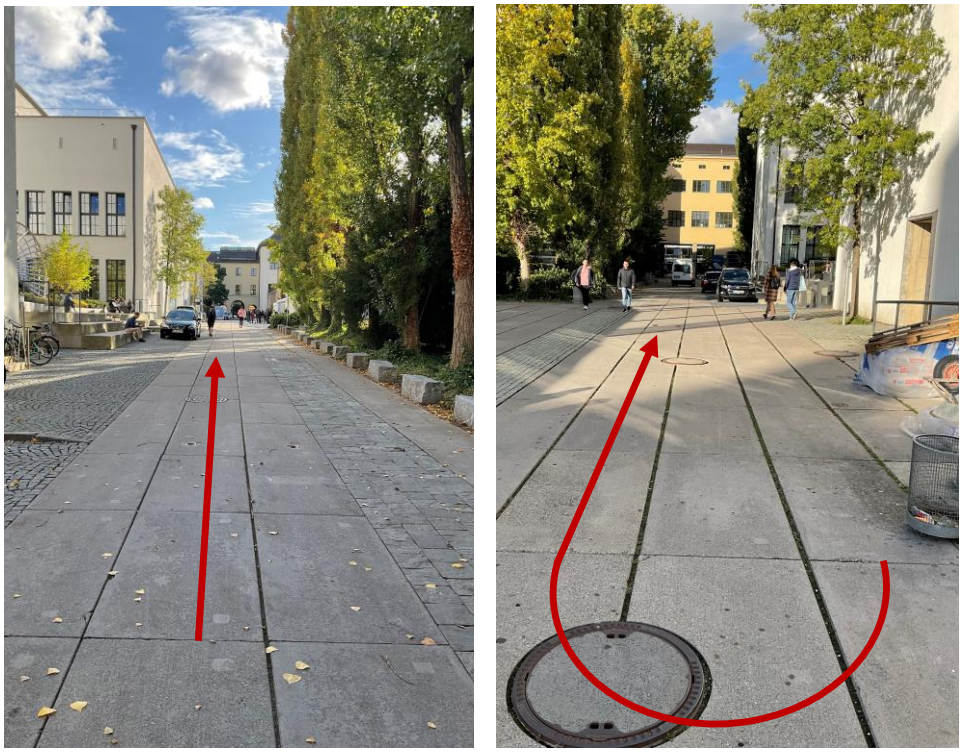

Fig. 2: Test track for the different experimental setups

Results and Discussion

The following section presents the results of the experiments. Subsequently, limitations and suitabilities of the sensor alignments and settings for the discussed applications are presented, as tested with the discribed experimental setups.

Frontal Sensor Alignment

Experiments were conducted with a frontal sensor alignment (see Fig. 1 (a), Position 1) with two different sensor resolutions. These resolutions vary depending on the densities of the generated point clouds. A distinction is made between low and high resolution, while a moderate speed level was kept for each case (see Tab. 1).

Fig. 3 shows the point clod generated with frontal sensor alignment and high resolution.

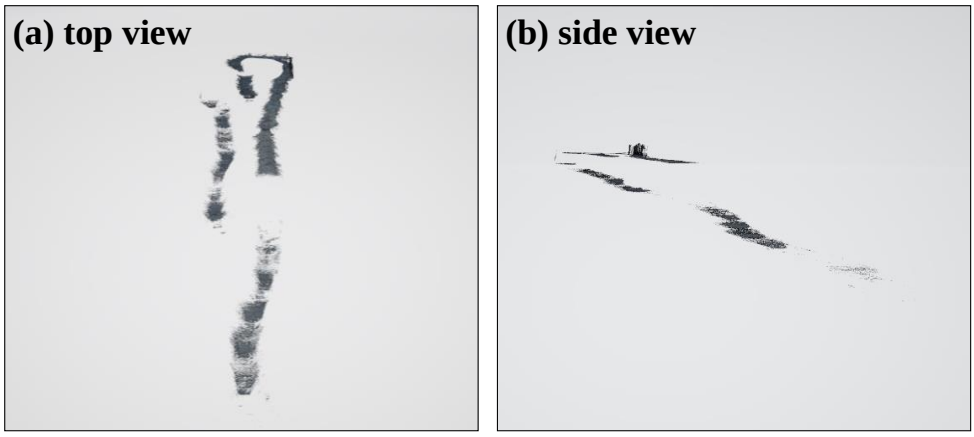

Fig. 3: Point cloud generated with frontal sensor alignment and high resolution

The generated point cloud shows an incomplete mapping of the infrastructure with a low coverage of the mapped road space (a) as well as an incorrect representation of its altitude (b). In addition, it was observed that a frontal sensor alignment did not allow the detection of objects located next to the mapped road space, while the high resolution sensor setting caused the data acquisition to stop due to the high file size resulting from the density of the generated point cloud.

Therefore, a low-resolution sensor setting was tested for the suitability of the discussed applications. Fig. 4 shows the point cloud generated with frontal sensor alignment and low resolution.

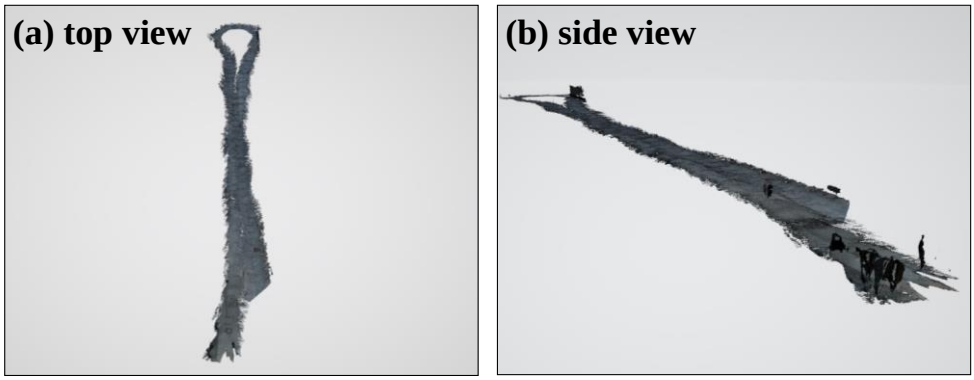

Fig. 4: Point cloud generated with frontal sensor alignment and low resolution

While the point cloud generated with low resolution still shows an incomplete mapping of the infrastructure as well as a not entirely accurate representation of its altitude, it reveals, compared to the previous experimental setup (see Fig. 3), a higher coverage of the mapped road space (a) and a more precise mapping of its flat altitude (b). In addition, it was observed that a frontal sensor alignment with low resolution did also not allow the complete detection of objects located next to the mapped road space, while it enabled data acquisition in one run.

Lateral Sensor Alignment

Since the detection of objects located next to the mapped road space is not possible with a frontal sensor alignment, experiments were conducted with different lateral sensor alignments. A low resolution was kept in each case, with the sensor alignment being distinguished between a fully lateral and a partially lateral orientation (see Fig. 1 (a), Position 2 + Position 3 respectively). In addition, the experiments with partially lateral sensor orientation were conducted with different speed levels. It is dinstinguished between a moderate and a low speed level (see Tab. 1).

Fig. 5 shows the point cloud generated with fully lateral sensor alignment, low resolution and a moderate speed level.

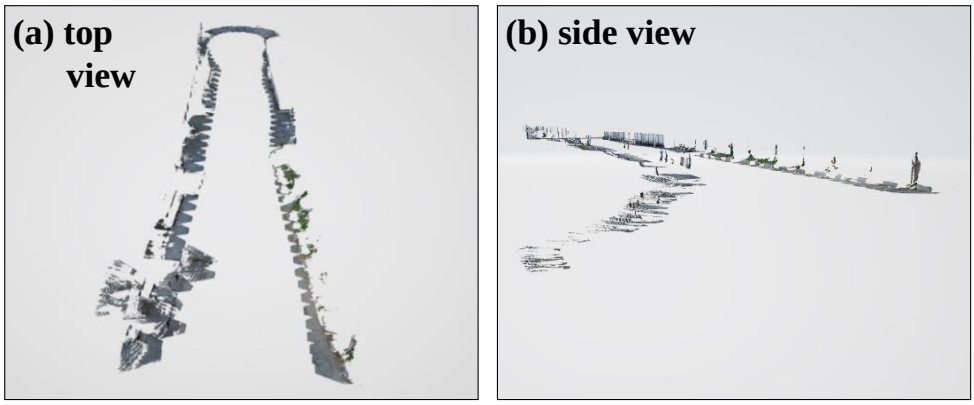

Fig. 5: Point cloud generated with fully lateral sensor alignment, low resolution and moderate speed level

The experiments with a fully lateral sensor alignment resulted in an incomplete mapping of the infrastructure with a low coverage and an undulating representation of the road space (a) as well as an incorrect representation of its altitude (b). In addition, it was observed that a fully lateral sensor alignment allowed the partial detection of objects located next to the mapped road space, although not all objects were captured.

Since the fully lateral sensor alignment showed significant limitations in terms of infrastructure mapping and detection of objects located next to the road space, a partially lateral sensor alignment has been tested. Fig. 6 shows the point cloud generated with partially lateral sensor alignment, low resolution and a moderate speed level.

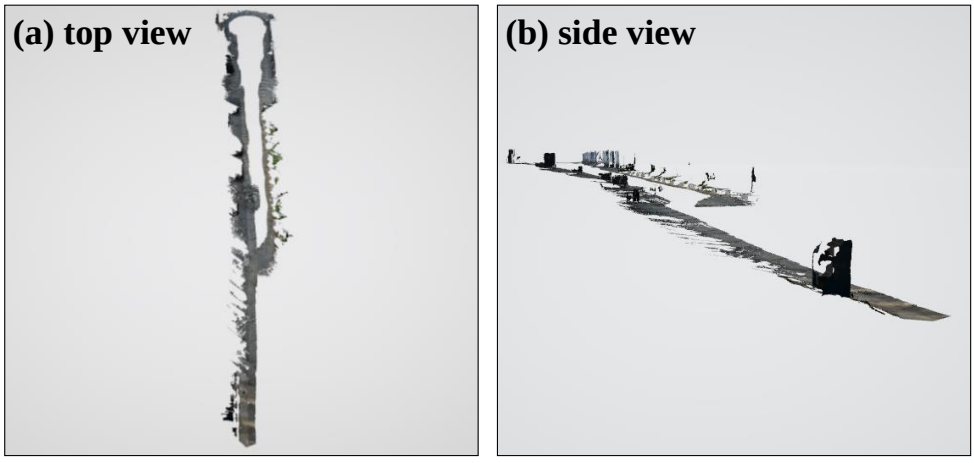

Fig. 6: Point cloud generated with partially lateral sensor alignment, low resolution and moderate speed level

While the point cloud generated with a partially lateral sensor alignment still shows an incomplete mapping of the infrastructure as well as a not entirely accurate representation of its altitude, compared to the previous experimental setup (see Fig. 5), a higher coverage of the mapped road space (a) and a more precise mapping of its flat altitude (b) could be observed. In addition, the partially lateral sensor alignment allowed the detection of objects located next

to the road space to a great extent. While detecting the presence of objects next to the road space, the sufficient mapping of its shape and thus the recognition of the objects' types was not possible with a moderate speed level of approximately 15 km/h.

Therefore, experiments with a partially lateral sensor alignment and low speed level of approximately 5 km/h were conducted. Fig. 7 shows the point cloud generated with partially lateral sensor alignment, low resolution a low speed level.

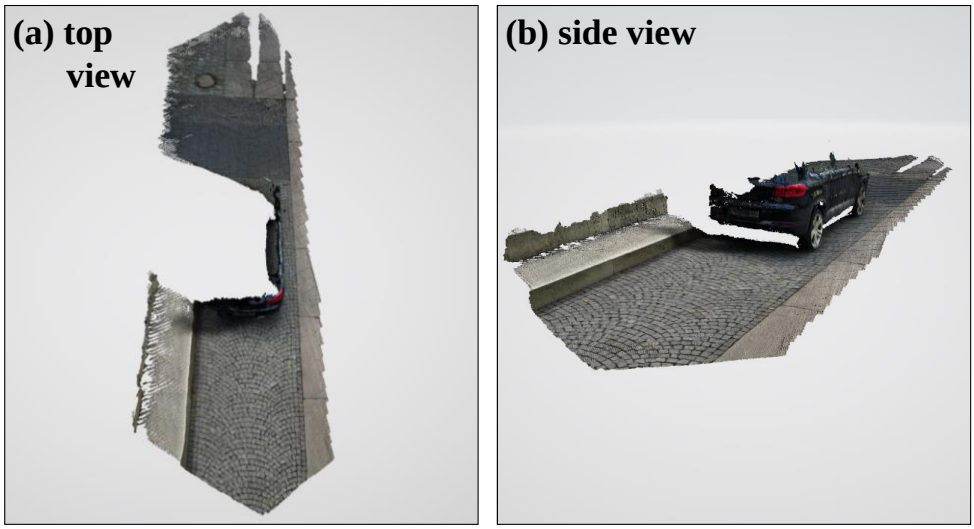

Fig. 7: Point cloud generated with partially lateral sensor alignment, low resolution and low speed level

The experiments conducted with a partially lateral sensor alignment and a low speed level show a complete mapping of the infrastructure (a) as well as an accurate representation of its flat altitude (b). Furthermore, all objects located next to the mapped road space were detected and its shapes were accurately mapped (e.g. parked vehicles and stairs). The infrastructure located behind objects adjacent to the road space could not be mapped due to the occulation of the sensor ray.

Swivelling Sensor Alignment

In addition to experiments with a frontal and different lateral sensor allignments, experiments with a swivelling sensor allignment (frontal sensor alignment with lateral oscilation, see Fig. 1 (a), Position 4) were conducted. A low resolution was kept in each case, with a distinction being made between a static and a dynamic case. While for the static case the point cloud generation was conducted once at standstill, the dynamic case was performed at a low speed level (approx. 5 km/h).

Fig. 8 shows the point cloud generated with swivelling sensor alignment and low resolution for the static case.

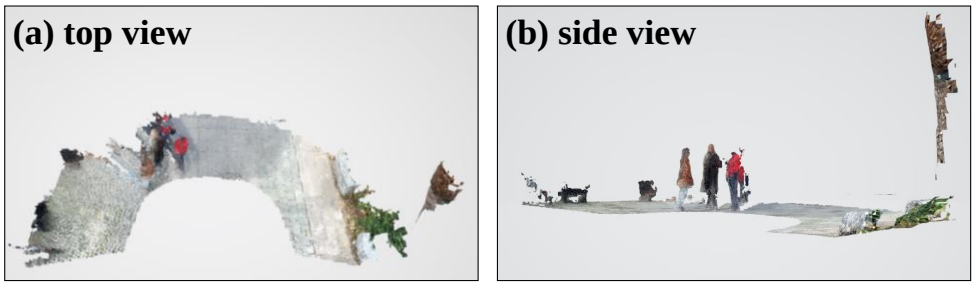

Fig. 8: Point cloud generated with swivelling sensor alignment and low resolution for the static case

In the static case of the swivelling sensor alignment, a point cloud was generated showing a complete mapping of the infrastructure not occluded by objects adjacent to the road space (a), as well as an accurate representation of its flat altitude (b). In addition, all objects located next to the mapped road space were detected and its shapes were accurately mapped (e.g. pedestrians and vegetation).

While for the static case of the swivelling sensor alignment, the point cloud generation was conducted once at standstill, the data acquisition for the dynamic case was conducted with a constant low speed level. Fig. 9 shows the point cloud generated with swivelling sensor alignment and low resolution for the dynamic case.

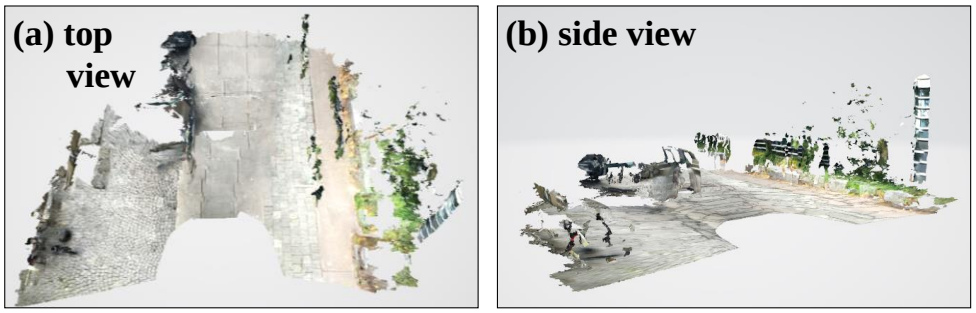

Fig. 9: Point cloud generated with swivelling sensor alignment and low resolution for the dynamic case

The point cloud generated for the dynamic case of the swivelling sensor alignment shows a distorted representation of the mapped infrastructure and objects located next to it (a), while the flat altitude was captured accurately (b). It was observed that the combination of constant forward moving and continuous lateral oscilation of the sensor resulted in partial reflection of the sensor rays and thus inaccurate representation of the road space and adjacent objects (e.g. pedestrians, cars).

Perpendicular Sensor Alignment

In addition to the experiments on general infrastructure mapping, experiments on the precise detection of infrastructural damages were conducted. The experiments were conducted with a (semi-)perpendicular sensor alignment (see Fig. 1 (b)) and low resolution in each case. A distinction was made between a static and a dynamic case. While for the static case the point cloud generation was conducted at standstill and fully perpendicular sensor alignment, the dynamic case was performed at a low speed level (approx. 5 km/h) and semi-perpendicular sensor alignment. The static case was performed for both a pothole and a street bump, while the dynamic case was performed solely for a pothole.

Fig. 10 shows the point cloud of a pothole generated with a fully perpendicular sensor alignment for the static case.

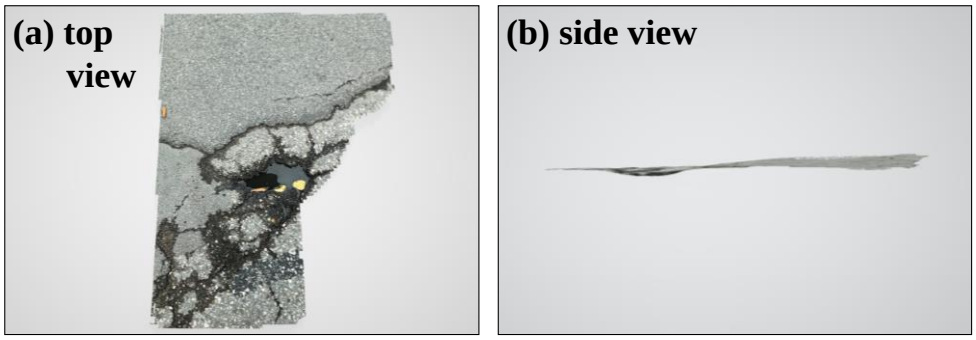

Fig. 10: Point cloud of a pothole generated at standstill with fully perpendicular sensor alignment

The point cloud of the pothole generated for the static case shows a precise representation of the shape of the pothole and the adjacent street space (a) as well as its depth (b).

Furthermore, the static case was performed for a street bump. Fig. 11 shows the point cloud of a street bump generated with a fully perpendicular sensor alignment for the static case.

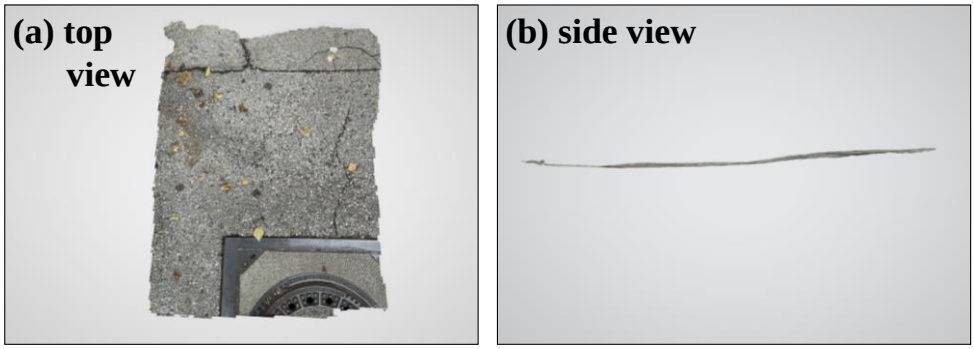

Fig. 11: Point cloud of a street bump generated at standstill with fully perpendicular sensor alignment

Also for the street bump, the generated point cloud shows an accurate representation of its shape and the adjacent street space (a) as well as its altitude (b).

In addition to the static case of the perpendicular sensor alignment, the point cloud generation of a pothole was conducted with a constant low speed level of approximately 5 km/h and a semi-perpendicular sensor alignment. Fig. 12 shows the point cloud generated with a semi-perpendicular sensor alignment for the dynamic case.

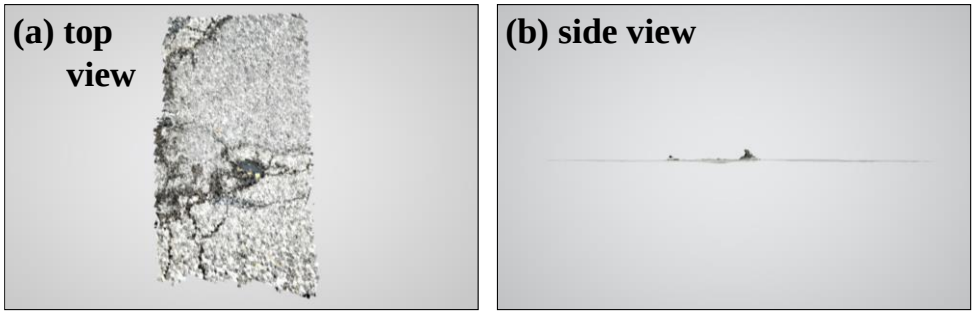

Fig. 12: Point cloud of a pothole generated at low speed level with semi-perpendicular sensor alignment

Compared to the previous experimental setup for the mapping of infrastructural damages (see Fig. 10), the point cloud of the pothole generated for the dynamic case shows a less precise representation of the shape of the pothole and the adjacent street space (a) as well as a less accurate mapping of its depth (b).

Limitations and Possible Applications

The following section sumarises the results of the different experimental setups. While the test characteristics divide into those mentioned in the methodology (see Tab. 1), the results of the experimental setups are summarised according to the accuracy of different performance indicators of interest. A qualitative scale is used to evaluate the performance indicators: good (green), moderate (yellow), low (red).

Tab. 2 sumarized the results for the experimental setups with a bicycle-mounted sensor.

Test Characteristics			**Accuracy**			
Sensor Alignment	**Resolution**	**Speed Level**	**Infrastructure mapping**	**Altitude representation**	**Adjacent object detection**	**Mapping of adjacent objects**
Frontal	High	Moderate				
	Low					
Fully Lateral						
Partially Lateral						
		Low				
Dynamic Swivelling						
Static Swivelling		Stationary				

Tab. 2: Summary of results for the experimental setups with a bicycle-mounted sensor

The summary of results for the experiments performed with the bicycle-mounted sensor show good accuracy for all performance indicators of interest for a partially lateral sensor alignment, low resolution and a low speed level on the one hand, and the static case for the swivelling sensor alignment with low resolution on the other hand. Due to the significantly higher time need for infrastructure mapping with the static case of the swivelling sensor alignment, compared to the partially lateral sensor alignment at a contant low speed level, the practicability of the swivelling sensor alignment needs to be evaluated individually for possible future applications.

One interesting application of bicycle-mounted sensors is the development of an interface to urban digital twins that might be fed with crowd-sourced mobile sensor data. Furthermore, the high accuracy in adjacent object detection and mapping of its shape would enable several applications in the research area of moving observers, that use data outside the ego-vehicle perspective for several applications in e.g. traffic engineering or the smart city context.

The remaining experimental setups showed moderate or low accuracies for several performance indicators of interest. It was observed that a high resolution of the generated point cloud causes the data acquisition to terminate early due to the file size resulting from the high density of the generated point cloud. Furthermore, it has shown that a moderate speed level of approximately 15 km/h leads to partial reflections of the sensor rays and thus inaccuracies in the performance indicators of interest.

Tab. 3 sumarized the results for the experimental setups with a handheld sensor.

Test Characteristics			Accuracy	
Sensor Alignment	**Resolution**	**Speed Level**	**Infrastructure damage mapping**	**Altitude / depth representation**
Dynamic, Semi-Perpendicular	Low	Low		
Static, Fully Perpendicular				

Tab. 3: Summary of results for the experimental setups with a handheld sensor

The summary of results for the eperiments conducted with the handheld sensor show good accuracy for both performance indicators of interest for the static and fully perpendicular sensor alignment. The dynamic and semi-perpendicular sensor alignment, on the other hand, revealed moderate accuracies for the performance indicators due to partial reflections of the sensor ray resulting from the constant movement during data acquisition.

Accurate mapping of infrastructural damages with sensors encorporated in mobile devices enables a crowd-sourcing option for urban data mining that could expand the database for municipalities and cities in decision making on maintenance options for VRU infrastructure. Furthermore, an interface to urban digital twins could add a local and highly detailed component to the amount of information collected, bringing significantly more value to such applications.

Conclusion

In this work, various experiments were conducted to test the suitability of the LiDAR sensor built into the Apple iPad Pro 2020 (and iPhone 12 Pro) for mobile mapping of VRU infrastructure. The tests have shown that the results are thoroughly usable. The decisive factors have proven to be the combination of a low speed level and a low resolution of the point clouds. In addition, the sensor alignment is crucial, which should be adapted to the scan target. The resulting high-quality data acquisitions prove the suitability of low-cost LiDAR sensors installed in mobile devices for various applications that normally use conventional sensor systems at high purchase and maintenance costs.

With these results, various applications are conceivable, like the integration of these outcomes as a state description in urban digital twins. In the smart city context, information could be used as a monitoring application through crowd sourcing from citizens which would expand the decision making basis for municipalities and cities in the context of maintenance options for VRU infrastructure. Furthermore, various applications in the research area of moving observers, collecting and using data outside the ego-vehicle perspective for e.g. traffic engineering and control purposes or further concepts in the smart city context, are conceivable. These applications will be verified and tested in future work building on this study.

Acknowledgement

The authors confirm contribution to this study as follows:

Study conception and design: M. Ilic, J. Vogt; data collection: J. Vogt, M.Ilic; analysis and interpretation of results: M. Ilic, J. Vogt; draft manuscript preparation: M. Ilic, J. Vogt; supervision: K. Bogenberger

All authors reviewed the results and approved the final version of the manuscript.

References

APPLE., 2020: Apple unveils new iPad Pro with LiDAR Scanner and Trackpad Support in iPadOS. https://www.apple.com/de/newsroom/2020/03/apple-unveils-new-ipad-pro-with-lidar-scanner-and-trackpad-support-in-ipados/. Accessed February 25, 2022.

DUMMER, M., JOHNSON, K., ROTHWELL, S., TATAH, K., & HIBBS-BRENNER, M., 2021: The role of VCSELs in 3D sensing and LiDAR. SPIE Optical Interconnects XXI.

GOLLOB, C., RITTER, T., KRASSNITZER, R., TOCKNER, A., & NOTHDURFT, A., 2021: Measurement of Forest Inventory Parameters with Apple iPad Pro and Integrated LiDAR Technology. MDPI - remote sensing, Volume 13: 3129 - 3164.

LUETZENBURG, G., KROON, A., & BJØRK, A. A., 2021: Evaluation of the Apple iPhone 12 Pro LiDAR for an Application in Geosciences. Nature, Volume 11: 1 - 9.

PUENTE, I., GONZÁLEZ-JORGE, H., ARIAS, P., & ARMESTO, J., 2011: Land-Based Mobile Laser Scanning Systems: A Review. ISPRS - International Archives of the Photogrammetry Remote Sensing and Spatial Information Science, Volume 38: 163 - 168.

RANGWALA, S., 2020: Forbes. The iPhone 12 - LiDAR At Your Fingertips. https://www.forbes.com/sites/sabbirrangwala/2020/11/12/the-iphone-12lidar-at-your-fingertips/. Accessed March 01, 2022.

SPREAFICO, A., CHIABRANDO, F., LOSÈ, L. T., & TONOLO, F. G., 2021: The iPad Built-In LiDAR Sensor: 3D Rapid Mapping Test And Quality Assessment. The International Archives of the Photogrammetry: Remote Sensing and Spatial Information Sciences, Volume 43: 63 - 69.

TAVANI, S., BILLI, A., CORRADETTI, A., MERCURI, M., BOSMAN, A., CUFFARO, M., .CARMINATI, E., 2021: Smartphone assisted fieldword: Towards the digital transition of geoscience fieldwork using LiDAR-equipped iPhones. Elsevier - Earth Science Reviews, Volume 227: XXX - XXX.

VOGT, M., RIPS, A., & EMMELMANN, C., 2021: Comparison of iPad Pro®'s LiDAR and TrueDepth Capabilities with an Industrial 3D Scanning Solution. Technologies 2021. MDPI - remote sensing, Volume 9: 25 - 38.